A threshold based earthquake early warning system for offshore events in Southern Iberia

M. Picozzi[(1)], S. Colombelli[(1,2)], A. Zollo[(1)], M. Carranza[(3)], and E. Buforn[(3)]

1 Dept. Physics, Università Federico II, Naples, Italy

2 RISSC-Lab, AMRA scarl, Naples, Italy

3 Dept. Geofisica y Meteorogia, Univesidad Complutense, Madrid, Spain

Abstract

The south of the Iberian Peninsula is a region situated at the convergence of the Eurasian and African plates. This region experiences large earthquakes with a long separation in time, the best known of which is the great 1755 Lisbon Earthquake (i.e., maximum macroseismic intensity, I_{max}=X), which occurred SW of San Vicente Cape (SW Iberian Peninsula). The high risk of damaging earthquakes has recently lead Carranza et al. (2013) to investigate the feasibility of an EEWS in this region. The analysis of the geometrical situation between the Iberian seismic networks and the San Vicente Cape area led the authors to conclude that a threshold-based approach, which would not require the real-time location of the earthquake, might be the best option for EEWS in SW Iberia. The current work explores this hypothesis, and proposes a new EEW approach that extends the standard P-wave threshold based single station analysis to the whole network. The proposed method allows the real-time estimation of the potential damage at stations that are triggered by P-waves, as well as at the not-triggered ones, giving the advantage of a greater lead-time for the release of alerts. Results of tests made with synthetic data mimicking the scenario of the great 1755 Lisbon Earthquake, and those obtained by applying the new approach to available recordings, indicate that an EEW estimation of the potential damage associated with an event in the San Vicente Cape area can be obtained for a very large portion of the Iberian Peninsula.

1. Introduction

An Earthquake Early Warning System (EEWS) is a real-time system integrating seismic network and software capable of performing a real-time data telemetry and analysis in order to provide alert messages to users within seconds from the begin of an earthquake and certainly before that the S-waves generated by the event reach the users.

The use of EEWS to reduce the exposure of population to seismic risk is nowadays increasing and several countries around the world have already developed EEWS, or are on the verge of doing so. Japan, Taiwan, Mexico and California, for example, already have operational EEWSs (Horiuchi et al., 2005, Wu and Zhao, 2006, Espinosa-Aranda et al., 2009, Böse et al., 2009, Böse et al., 2007). EEWSs are also under development and testing in other regions of the world, such as Italy, Turkey and China (Satriano et al., 2010; Zollo et al., 2014, Alcik et al., 2009, Peng et al., 2011). Finally, a feasibility study is in progress in Spain (Carranza et al., 2013).

Most EEWS are designed as either “regional”, “on-site“ or “front-detection” systems. The selection of the configuration of the EEWS essentially depends on the network geometry and on the source-to-site distance.

A regional warning system is based on a dense sensor network of stations deployed in the vicinity of a source region, while sites to be alerted are generally far away from it. In this configuration, the earthquake location and magnitude are estimated using the early portion of the recorded signals and the peak ground motion at distant sites (Peak Ground Velocity – PGV - or Peak Ground Acceleration - PGA) is then predicted using empirical ground-motion prediction equations (e.g., among others, PRESTo in Southern Italy; Iannaccone et al., 2010; Satriano et al., 2011).

Site-specific (or onsite) EEWS consist of a single sensor deployed in the proximity of the target structure that is to be alerted. In this configuration, the earthquake early warning (EEW) parameters measured in the very first seconds of the P-wave are used to predict the final peak ground motion at the same site, without locating the event or estimating its magnitude (e.g., among others, the τc-Pd Onsite algorithm in California; Böse et al., 2009; Böse et al., 2012).

The "front detection" approach consists of an array of seismic sensors between the potential source area and the target area. Such a system requires prior knowledge of the possible location of earthquake sources, but, depending on their distance from the target area, it can then provide quite long warning or lead times (i.e., tens of seconds) before the arrival of destructive waves. An example of a front detection system is the Seismic Alert System (SAS) for Mexico City (Espinosa-Aranda et al., 1995), based on a linear array of sensors along the coast designed to detect earthquakes from the offshore subduction zone and to issue the warning to Mexico City.

Integrated approaches have also been proposed. The idea here is to jointly use both locally measured parameters and predicted ground motion values at regional scale. The integrated approaches are likely to provide reliable estimates of source parameters and a rapid prediction of the Potential Damage Zone (PDZ) resulting from the earthquake (i.e., the area in which most of the damage is expected to occur) and to define local alert levels (Zollo et al., 2010; Colombelli et al., 2012a).

Whichever configuration is adopted, earthquake magnitude or peak ground motion estimations for early warning applications are based on empirical relationships relating the earthquake’s size to parameters measured in the early portion of the P and S-wave trains (e.g., see among others, Kanamori, 2005). In the context of real-time applications, different amplitude and period parameters have been proposed to obtain independent estimates of the earthquake’s magnitude. As for the ground shaking predictions, which is generally

described by a single parameter (PGA or PGV), several authors have demonstrated that the maximum amplitude of the initial P-wave displacement (e.g., measured over the first 3 seconds) can be used as a proxy for the resulting PGV at the same site (Kanamori, 2005; Wu & Kanamori, 2005; Wu & Kanamori, 2008; Zollo et al., 2010).

The Iberian Peninsula is presently undergoing a NNW-SSE uniform horizontal compression resulting from the convergence of the Eurasian and African plates (Buforn et al., 1988a). The region situated at the plate boundary experiences large earthquakes with long return periods (Buforn et al., 1988b), and thus is of particular interest for an EEW study. The area of S. Vicente Cape (SVC, SW Iberia, Fig. 1) has generated large shocks, including the damaging 1755 Lisbon Earthquake (i.e., maximum macroseismic intensity, I_{max}=X), and, more recently, the Ms 8.1 1969 S. Vicente Cape earthquake, both of which generated tsunamis. Moderate-to-strong earthquakes have also occurred in the Gulf of Cádiz (GC, Fig. 1), an example being the Ms 6.1, 1964 event. However, in this area, even smaller magnitude earthquakes can cause considerable panic and fear among the population, since they are felt over an extensive region, as was the case with the December 2009 earthquake (Mw=5.5), which was felt over a major part of the SW of the Iberian Peninsula, and as far away as its center (Pro *et al*., 2013).

Carranza et al. (2013) investigated the feasibility of an EEWS in these regions of the Iberian Peninsula, taking into account the limitation of the existing seismological networks. The geometrical situation between the Iberian seismic networks and the SVC and GC seismogenic zones makes it difficult to obtain an early and reliable location of the epicenter. For this reason, Carranza et al. (2013) suggested that a threshold-based approach, which would not require the real-time location of the earthquake, might be the best option for an EEWS in SW Iberia. To better highlight this issue, we computed synthetic P-wave arrival times (corrupted by random noise with 1 second standard deviation) for a scenario mimicking the 1755 Lisbon Earthquake. Then, we tried to locate

the event considering different numbers of stations and using the RTLoc algorithm of Satriano et al. (2008), one of the most robust algorithms developed within the EEW community. Figure (2a) shows that when only the first three stations are used, the estimated location can be completely wrong. Figures (2b and c) in turn show that the location found using ten stations considering two sets of arrival times varies as a function of the random noise added to the data. The latter examples, in particular, highlight that in this geometrical arrangement, and using a limited number of stations (which is a requirement in EEW operations), the inferred location is not reliable.

In this work, we explore the hypothesis proposed by Carranza et al. (2013). In particular, we propose a new EEW approach that extends the standard on-site single station analysis scheme to the whole network. The goal of the new approach is to estimate the potential damage at both stations that triggered on P-waves, as well as at the not-triggered stations. We exploit the EEW relationships derived by Carranza et al. (2013) for SW Iberia. However, with respect to that study, where only recordings from seismic stations with broad-band sensors were used, here we also considered strong motion stations (i.e., those of the Instituto Geográfico National (IGN), Western Mediterranean (WM), and Portuguese National (IP) networks), for a total of 112 stations, under the assumption that their hardware characteristics allow for real-time data telemetry. Furthermore, we also assume that this seismic network would be managed at a main center, similarly to the ISNet network (Iannaccone et al., 2010), where the real-time data analyses necessary for EEW approach proposed in this study would occur.

2. San Vicente Cape and Gulf of Cádiz seismogenic zones

The San Vicente Cape (SVC) and Gulf of Cádiz (GC) seismogenic zones (Figure 1) extend from 12ºW to 6.5ºW, and from 35°N to 37.5°N. A large number of papers have described these zones, which are of great interest due to their tectonic complexity and being the location of the occurrence of the great 1755 Lisbon Earthquake (Fukao, 1973; Udías et al., 1976; Grimison and Chen, 1988; Buforn et al., 1988a; Morel and Megharoui, 1996; Hayward et al., 1999; Fernández-Ibañez et al., 2007; Stich et al., 2007; Pro et al, 2013). In Buforn et al, (2015, this volume), there is a detailed description of the largest earthquakes that have occurred in this region. The region's main characteristics may be described as follow (Figure 1). Earthquakes are associated with the plate boundary between Eurasia and Africa, well defined at its western part, from the Azores Islands to 12ºW. Along this longitude, a transition starts from an oceanic to a continental plate boundary. A consequence of this transition is that seismicity spreads over a wide area and the plate boundary is not well defined, corresponding to a wide deformation zone that also includes the region south of Iberian Peninsula and northern Morocco.

Most of the epicenters within this zone are located offshore with three main concentration of earthquakes (Figure 1). The first one is located at the western part of the region, at the Gorringe Bank (GB), showing a NE-SW direction in agreement with the trend of this structure. The second concentration is at the Horsenhoe Scarp (HS), where the 1969 (Mw=7.8) and 2007 (Mw=5.9) earthquakes occurred. This is one of the hypothetical locations of the epicenter of the 1755 Lisbon Earthquake. The third concentration corresponds to the Gulf of Cadiz (GC) where the 1964 earthquake (Ms=6.1) occurred. On land, there are some concentrations of earthquakes on both sides of the Strait of Gibraltar (SG), but with moderate magnitudes, generally less than 5.0.

Another characteristic of the earthquakes in these zones is their focal depth. Most epicenters correspond to shallow events (h<40km), but there are also earthquakes at intermediate depths (40<h<150km, Figure 1). Due to the bad azimuthal coverage of the seismic stations, determinations of focal depths are not well constrained and this intermediate depth seismicity is uncertain (Buforn et al., 2004). However, it is important to note that for the 1969 and 2007 earthquakes, focal depths obtained from the inversion of body waves and slip distributions are between 30 and 40 km, while in the GC, the 1964 shock had a shallow focus (12km).

Focal mechanisms of large earthquakes in the SVC and GC (1969, 2007 and 1964) correspond to a thrusting motion leading to a horizontal pressure axis oriented in the NNW-SSE direction, a consequence of the collision between Eurasian and African plates.

3. Methodology

3.1. Overview

Figure (3) presents the outline of the EEW procedure we have designed with the goal of mitigating the seismic risk arising from the S. Vicente Cape area. As discussed in the previous section, given the geometrical relationship between the S. Vicente Cape source area and both the seismic network and cities' distribution (i.e., the EEWS's targets), we opted for a threshold-based EEW approach, which aims to predict the potential damaging effects of an offshore earthquake by the real-time analysis of signals recorded by coastal stations without any need for accurate estimations of the earthquake's location and magnitude. The procedure is composed of two main parts.

The first one consists of a classical single station on-site approach (SOS). The empirical scaling relationship between the initial peak ground displacement (Pd) and the final Peak Ground Velocity (PGV) at each recording site is one of the most stable and robust

correlations employable for EEWS (Wu and Kanamori 2005; Wu and Kanamori 2008a; Wu and Kanamori 2008b; Zollo et al. 2010). The Pd is typically measured in a 3-seconds window after the first P-wave arrival. Colombelli et al. (2012b) and (2014) recently showed that an expanded P-wave time window should be used to overcome the Pd saturation effect in case of large earthquakes (i.e., M>7; e.g., among the others, Rydelek and Horiuchi 2006; Rydelek et al., 2007; Zollo, Lancieri, and Nielsen 2007).

We apply the log Pd vs PGV empirical relationship derived by Carranza et al. (2013). Then, the PGV predicted from Pd (PGV_{3sec}) is in turn converted to a Modified Mercalli Intensity (I_{MM}) by the empirical regression proposed by Wald et al., (1999), which is implemented by the USGS in the ShakeMap tool for the rapid estimation of strong ground shaking after a damaging earthquake. Thus, the potential damaging effects of a moderate-to-large earthquake can be rapidly predicted by Pd measurements using the correlation of this parameter with PGV. Hence, as proposed by Zollo et al. (2010) and Colombelli et al. (2012a), the I_{MM} derived from the recorded P-waves can be used to deliver a potential damage zone (PDZ) map. Applying such a SOS approach, the estimation of I_{MM} is possible only at stations already triggered on the P-waves.

In order to also obtain a prompt estimation of the potential damage at sites not yet reached by the P-waves, we propose here an approach where the information derived by the SOS scheme is integrated with information describing the geometrical relationship between triggered and not-triggered stations. We term the second procedure the Network-based On-Site approach (NOS), which aims at the prediction of I_{MM} at not-triggered stations.

As shown in Figure (3), the SOS approach is adopted whenever another station is triggered and a local P-wave prediction of the final I_{MM} at that site is derived. The procedure continues delivering evolutionary maps of the predicted shaking at the station sites until no more not-triggered stations are left. Following Zollo et al. (2010), the I_{MM} maps can be used to derive the PDZ. Whenever coastal stations begin recording the S-

wave ground motion, these pieces of information can then be included within the NOS procedure for the prediction of the shaking at not-triggered stations at any other target of interest.

3.2 Network-based On-Site (NOS) approach

For the scenarios of offshore earthquakes, the network-based on-site (NOS) approach exploits the real time information from triggered and not-yet-triggered stations to constrain the direction of the propagation of the P-wavefront (Figure 4a), and therefore the epicenter back-azimuth. For this purpose, a simplified version of the RTLoc algorithm of Satriano et al. (2008) has been adopted. The information provided at a given instant (t_{now}) during the initial stages of an earthquake, that is when the network status involves a few triggered stations and some not-triggered, can be used to compute the 'conditional' equal differential (EDT) surfaces (Font et al., 2004). As discussed by Satriano et al. (2008), these EDT surfaces are conditional because they are defined under the condition that for each pair of triggered and not-triggered stations, the latter will trigger at any time after the current clock time t_{now}.

Figure (4b, c, and d) show an application of this evolutionary procedure to synthetic data derived for a scenario having the epicenter corresponding to the 1755 Lisbon Earthquake. All the synthetic P-wave arrival times used in this work, which are necessary for the implementation of the RTLoc algorithm, have been computed for a 1D velocity model for the South Iberia region (IGN, 1983), with noise introduced consisting of a random perturbation with a standard deviation equal to one second. With the passing of time, the progressive increase in the number of triggered stations allows for the improvement of the identification of the region where the epicenter is most probably located. Then, knowledge

of the P-wavefronts' direction of propagation allows for the assessing of the interstation distances (D) between triggered and the un-triggered stations (Figure 4b), which in turn represents a fundamental piece of information for estimating the PGV at not-triggered stations. Since the true location of the epicenter is unknown, and in the cases of the SVC and GC areas their distance from the coast is large, the interstation distances are estimated under the assumption of planar wavefronts.

Similarly to what is done for the Pd in EEW procedures (e.g., among others, Zollo et al., 2006), the parameter PGV is related to the earthquake magnitude (M) and the hypocentral distance (R) through a standard ground motion prediction equation (GMPE):

$$\log_{10}(PGV) = A + B*M + C*\log_{10}(R) \quad (1)$$

where PGV is in centimeters per second, R is in kilometers, and A, B and C are constants to be determined by a multivariate linear regression analysis of the specific region's data.

The application of Eq. (1) within the NOS procedure to know the PGV at not-triggered stations is, however, not possible, given that R is not known.

However, based on the observed decay of PGV with the distance from the first triggered station (D), we propose the following attenuation model:

$$\log_{10}(PGV_{3sec})_D = So + C'*\log_{10}(D) \quad (2)$$

where C' is assumed to equal C (i.e., the validity of this assumption has been verified on available recordings, see Section 4 and Figure 5), and the term 'So' is determined in real time through the best-fit regression expressed in equation (2) using the PGV_{3sec} measured at the triggered stations and using their distances (D) measured along the wavefront's propagation direction from the first-triggered station.

Hence, when the wavefront's propagation direction is known, Eq. (2) can be used to estimate the PGV at not-triggered stations (PGV_{NT}). The procedure to estimate the factor (So) and the PGV_{NT} can start when at least two PGV values are available (i.e., two triggered stations), and is repeated every time another station triggers and its PGV_{3sec} value is available (Figure 5a). Therefore, like the azimuth determination, the PGV_{NT} estimation is also evolutionary, and continues until all the stations in the network have triggered (Figure 3).

At each time a new or updated PGV_{NT} estimate is available, the empirical regression law proposed by Wald et al. (1999) is applied to estimate the $I_{MM(NT)}$. Hence, a PDZ map, including the $I_{MM(3sec + NT)}$ values that cover the whole area monitored by the seismic network, is computed (Figure 3). Of course, with the passing of time, the NOS derived intensity map will evolve to include more observed S-wave and Pd derived PGV values.

In principle, the procedure can be easily extended to any EEW target of interest.

4. Application and preliminary results

We tested the above EEW procedure for the S. Vicente Cape area using both synthetic and real data. The use of synthetic data was necessary due to the lack of recordings of larger earthquakes (M>6) in the area under study. The available real recordings are in fact relevant to seven moderate earthquakes (i.e., M between 4.5 and 5.9; Table 1), which were the largest events among those considered by Carranza et al. (2013) to derive for the South Iberia Region the empirical scaling relationships between Pd, M and R, as well as between Pd and PGV.

Since we did not find in the literature a GMPE to compute the PGV at the epicentral distances of our interest (i.e., between 100 km and 600 km), we combined the

relationships derived by Carranza et al. (2013) into a new standard attenuation expression that relates PGV with M and R (see Eq.1):

$$\log_{10}(PGV) = - 2.76 + 0.887*M - 1.479 *\log10(R) \quad (3)$$

As an example, Figure (6a) shows as examples the comparison between Eq. (3), together with curves representing plus and minus one standard deviation, and the PGV measured for the event #6 in Table (1). Figures (6b and 6c) show, for all the events considered in this study (Table 1), that the prediction errors (i.e., the logarithm of the ratio between the predicted and observed PGV values) plotted against epicentral distance (b), as well as in the relevant histogram (c), are stable over time, showing a maximum variability of about +/- 1, which is comparable to the usually encountered fluctuations in standard GMPEs (e.g., Akkar and Bommer, 2007). These results suggest that the distance attenuation coefficient of Eq. (3) can be used to predict the PGV at large distances within the Iberia region using Eq. (2) and following the procedure described in Section 3.2.

Figure (5b) shows the PGV observation for event #6 (Table 1) plotted both with respect to their epicentral distances and their interstation distances, together with the curves from Eq. (3) and Eq. (2), whose parameters have been found following the procedure of Section 3.2. For the same data, Figure (5c and d) shows the comparison between the observed and predicted PGV (i.e., from Eq. 2) values and the prediction errors against the interstation distance. These results indicate that Eq. 2 and the procedure of Section 3.2 allow for the prediction of reliable PGV_{NT} values, despite not knowing the epicentral distance.

4.1 Synthetic data scenario

In order to perform a first validation of the EEW procedure for a scenario mimicking the ground motion associated with the great 1755 Lisbon Earthquake (Mw 8.7), we used synthetic data. The input data are Pd values computed using the relationship derived by Carranza et al. (2013) considering the epicentral location and magnitude associated with this historical event (Johnston, 1996; Martínez Solares and López Arroyo, 2004), and the present network configuration (Figure 2). In order to make the feasibility tests more realistic, the Pd values are randomly noised considering the standard deviation associated with the relationship, and hence, they are expected to represent the actual ground motion variability in the real data.

Figure (7a) shows the map of reference intensities derived by the PGV from Eq. (3) for the location and magnitude of the 1755 Lisbon Earthquake scenario and the Wald et al. (1999) relationship. Figure (7b) shows the I_{MM} obtained by the application of the SOS and NOS procedures when the first three stations have triggered. For the sake of clarity, in all the following figures we have adopted a different formalism while drawing the I_{MM} for triggered and not-triggered stations (i.e., fully and contour colored symbols, respectively).

Furthermore, as an example, we have computed the lead-time for some Portuguese and Spanish target cities (Table 2, Figure 7a). In particular, the lead time has been computed as the S-wave arrival time at the target cities minus both the P-wave arrival time at a given triggered station (i.e., the 3rd, 10th, and 50th stations as in Figure 7b, d, and f) and a time of 2 seconds which is necessary for computation and data telemetry, which we assumed according to the experience with the PRESTo system at the ISNET accelerometric network in Southern Italy over a long period of testing (Satriano et al., 2010).

In the case of three triggered stations example (Figure 7b), the lead-time at the selected targets would potentially range between a minimum of 29 seconds for Portimao, and a maximum of 82 seconds for Seville (Table 2).

Figure (7c) shows the residual between the reference and the estimated I_{MM} values with respect to the inter-station distance. This result indicates that at this time, the estimation of the $I_{MM(NT)}$ is stable until about 200 kilometers from the triggered stations. For larger distances, the NOS procedure shows a bias towards smaller values by around three intensity units. However, by the time that ten stations have triggered (Figure 7d), the EEW I_{MM} map is more consistent with the reference one, with the residuals mostly confined within a range of +/- one intensity unit. In this case, given the large source-to-targets distance involved, the lead-time at the target cities is still large and ranges between 21 seconds for Portimao, and 73 seconds for Seville.

With the increase in the number of triggered stations, the EEW I_{MM} map relies much more on the PGV values derived from the SOS approach (i.e., from Pd values) and progressively improves its fit with respect to the reference one, of course at the price of a reduction in the lead-time. This is shown, for example, in Figures (7f and g), which are derived when considering fifty triggered stations, leading to no lead-time for Portimao, 5 seconds for Faro and 46 seconds for Seville.

4.2 Observed data analysis

The proposed EEW procedure was then applied offline to a set of recordings from seven small-to-moderate offshore earthquakes (Table 1). Of course, given their epicentral distances from the coast being of the order of one hundred kilometers, and having rather

low magnitudes (only in two cases larger than 5), the observed ground motion at the seismic stations is relatively small, and I_{MM} is less than V at all sites. In Figure (8), we present the results of the EEW analysis for the 2007 (M 5.9) event, which occurred in the S. Vicente Cape area (#3, Table 1). Interestingly, when using real data, after only three stations have been triggered, the EEW I_{MM} map is in agreement with the observed one according to the IGN (http://www.ign.es/ign/layoutIn/sismoDetalleTerremotos.do, last accessed on July 15, 2014). The resulting lead-times at the target cities range from 16 to 65 seconds (Table 3). In addition, despite their very low magnitudes, due to the different source origins, we also considered the cases of the M5.5 (#7) and M 4.7 (#1) events (Table 1), which occurred in the Gulf of Cadiz (Figure 9). Again in these cases, by the time that three and two stations, respectively, have triggered, we observe good agreement between the observed and predicted EEW intensity maps. Moreover, with only the exception of the city of Faro for event #1 (Figure 9f), the lead-time is still greater than zero (Table 3).

5. Discussion

In the previous section, we considered the SVC seismogenic region and presented a new EEW P-wave threshold-based approach for SW Iberia, where a classic Pd-PGV single-station analysis is extended to the whole network with the aim of deriving rapid PDZ map for the Iberian Peninsula.

The existing GMPEs are mostly limited to a distance range of one hundred kilometers (e.g., Akkar and Bommer, 2007, Bindi et al., 2010). However, in the case of great events, such as the 1755 Lisbon Earthquake, these relations are not appropriate for estimating the PGV at the large hypocentral distances in SW Iberia (i.e., mostly greater than two hundred

kilometers). For this reason, we exploited the EEW relationships derived by Carranza et al. (2013), which cover a distance range until six hundred kilometers, to derive a new PGV attenuation law (i.e., Eq.3). A limitation of this law, and therefore of the method we proposed, might be that the maximum magnitude of the events contained in the data set used by Carranza et al. (2013) was only 6.3. In our opinion, considering the high seismic risk of the Iberian Peninsula with respect to the occurrence of a great earthquake in the SVC region, the capability to predict the ground motion at large distances is an issue of primary importance that deserves further study.

With respect to such a seismic threat, we believe the most suitable EEWS for SW Iberia is a front-detection, threshold-based approach that exploits the information acquired at coastal stations to warn coastal sites and inland regions. As Carranza et al. (2013) and our study have shown, the early seconds of P-wave recordings can be used to obtain, in a very short time, robust prediction of the PGV at the recording stations. Information dealing with the expected ground shaking at these stations could then be communicated to the inland areas. Of course, due to the lack of knowledge about the event's location and magnitude, generally the estimation of the damage potential would be possible only for stations that recorded the P-waves and not for the others. With respect this issue, the procedure that we proposed in this work takes a step forward in allowing the prediction of the potential damage at stations that have not yet recorded the P-waves (i.e., using Eq.2), giving the advantage of a greater lead-time for the release of alerts. Furthermore, the method could be used to provide the potential damage estimation to any specified target area in the region.

We used synthetic data to mimic the scenario of the great 1755 Lisbon Earthquake. Our results indicate that by using only ten triggered coastal stations, a robust estimation of the potential damage, expressed as I_{MM}, can be obtained for a very large portion of the Iberian Peninsula. These results have been obtained using, as input data, Pd randomly extracted

from the regression between this parameter, M and R. Therefore, differently from real Pd values measured on short-time windows, our synthetic data do not suffer from the well-known saturation problem of EEW parameters. On the other hand, we are well aware that this issue cannot be ignored when real data are considered. Therefore, in order to be effective for great events, the procedure that we proposed should include the estimation of Pd from evolutionary increasing P-wave time windows as proposed by Colombelli et al. (2012b and 2014).

Despite the analyzed waveform data set including only low to moderate magnitude events, we consider the results from the application of our EEW procedure very encouraging. We have shown that already from the EEW information extracted from the first two or three triggered stations, reliable warnings accompanied by quite large lead-times can be released to rather large areas in the event of an earthquake in the SVC and GC seismogenic regions.

In our opinion, the use of increasing P-wave time windows, the validation of the GMPE for large distances considering larger magnitude event recordings, and an upgrade of all networks in the area towards a real-time data telemetry capability, are primary tasks for the realization of an effective front-detection EEWS in the Iberian Peninsula.

Acknowledgements.

We would like to thank K. Fleming for his comments and suggestions that allowed us to significantly improve the manuscript. K. Fleming kindly improved also the English. This work has been partially supported by MINECO, projects CGL2010-19803-C03-01 and CGL2013-45724-C3-1 and by the INNOCAMPUS project (Ministerio de Economía y Competitividad, Orden CIN/1934/2010), and the REAKT-Strategies and tools for Real Time Earthquake RisK ReducTion FP7 European project funded from the European Community's Seventh Framework Programme [FP7/2007-2013] under grant agreement n° 282862.

Table

Table 1. Main information of the recorded events with epicenters in the SVC and GC seismogenic regions considered in this study.

Id	Date	Time	Lat	Lon	Depth	Mw
1	10/01/2006	10:57:40	36.15	-7.71	40	4.7
2	21/06/2006	00:51:19	35.99	-10.63	40	4.9
3	12/02/2007	10:35:24	35.91	-10.46	30	5.9
4	10/05/2008	16:33:09	35.95	-10.75	40	4.7
5	22/05/2009	23:58:06	36.77	-9.79	40	4.5
6	05/07/2009	15:50:56	36.00	-10.48	35	4.5
7	17/12/2009	01:37:49	36.47	-10.03	35	5.5

Table 2. Lead-times at some Portuguese and Spanish target cities at the moment when different number of stations have triggered on P waves for the 1755 Lisbon Earthquake scenario (Figure 7).

City	**3 stations (s)**	**10 stations (s)**	**Lead-time 50 St. (s)**
Cádiz	73	65	38
Faro	41	33	5
Lisbon	43	35	8
Portimao	29	21	0
Seville	82	73	46

Table 3. Lead-times at some Portuguese and Spanish target cities for the M 5.9 (#3), M5.5 (#7) and M 4.7 (#1) events (Table 1; Figures 8 and 9).

City	**Ev. #3 (s)**	**Ev. #7 (s)**	**Ev. #1 (s)**
Cádiz	54	52	8
Faro	25	21	0
Lisbon	43	36	52
Portimao	16	9	7
Seville	65	62	27

References:

Akkar, S. and Bommer, J. J. (2007), Empirical Prediction Equations for Peak Ground Velocity Derived from Strong-Motion Records from Europe and the Middle East. Bulletin of the Seismological Society of America, Vol. 97, No. 2, pp. 511–530, April 2007, doi: 10.1785/0120060141

Alcik, H., O. Ozel, N. Apaydin, and M. Erdik M. (2009). A study on warning algorithms for Istanbul earthquake early warning system, Geophys Res. Lett. 36, L00B05, doi:10.1029/2008GL036659.

Bindi, D., L Luzi, M Massa, F Pacor. Horizontal and vertical ground motion prediction equations derived from the Italian Accelerometric Archive (ITACA). Bulletin of earthquake engineering 8 (5), 1209-1230.

Böse, M., Ionescu, C., & Wenzel, F. (2007). Earthquake Early Warning for Bucharest, Romania: Novel and revised scaling relations. Geophys Res Lett. 34, L07302.

Böse, M., Hauksson, E., Solanki, K., Kanamori, H. and Heaton, T.H. (2009). Real-time testing of the on-site warning algorithm in Southern California and its performance during the July 29, 2008 Mw 5.4 Chino Hills earthquake, Geophys Res Lett. 36 doi:10.1029/2008GL036366.

Böse, M., Heaton, T. & Hauksson, E. (2012). Rapid estimation of earthquake source and ground-motion parameters for earthquake early warning using data from single three-component broadband or strong-motion sensor, Bull. Seismol. Soc. Am., 102(2), pp. 738-750, doi: 10.1785/0120110152.

Buforn, E., A. Udías, and M. A. Colombás, (1988a). Seismicity, source mechanisms and seismotectonics of the Azores-Gibraltar plate boundary. Tectonophysics, 152, 89-118.

Buforn, E., A. Udías, and J. Mezcua, (1988b). Seismicity and focal mechanisms in south Spain. Bull. Seism. Soc. Am., 78, 2008-2224.

Buforn, E., M. Bezzeghoud, A. Udías, and C. Pro, (2004). Seismic sources on the Iberia-African plate boundary and their tectonic implications. Pure Appl. Geophys. 161, 623-646, DOI 10.1007/s00024-003-2466-1.

Carranza, M., E. Buforn, S. Colombelli, and A. Zollo (2013). Earthquake early warning for southern Iberia: A P wave threshold-based approach, Geophys. Res. Lett., 40, doi:10.1002/grl.50903.

Colombelli, S., Amoroso, O., Zollo, A. & Kanamori, H. (2012). Test of a Threshold-Based Earthquake Early Warning Using Japanese Data, Bull. Seism. Soc. Am., 102, 10.1785/0120110149.

Colombelli, S., A. Zollo, G. Festa, and H. Kanamori (2012). Early magnitude and potential damage zone estimates for the great Mw 9 Tohoku-Oki earthquake, Geophys. Res. Lett., 39, L22306, doi:10.1029/2012GL053923.

Colombelli, S., Zollo, A. Festa, G. and M. Picozzi. Evidence for a difference in rupture initiation between small and large earthquakes. Nat. Commun. 5:3958 doi: 10.1038/ncomms4958 (2014).

Espinosa-Aranda, J.M., A. Cuellar, A. Garcia, G. Ibarrola, R. Islas, S. Maldonado, and F.H. Rodriguez (2009). Evolution of the Mexican Seismic Alert System (SASMEX), Seism. Res. Lett. 80 694-706.

Espinosa-Aranda, J. M., A. Jiménez, G. Ibarrola, F. Alcantar, A. Aguilar, M. Inostrosa, and S. Maldonado (1995). Mexico City Seismic Alert System, Seism. Res. Lett., 66(6), 42–52

Fernández-Ibáñez, F., Soto, J.I., Zoback, M.D. y Morales, J. (2007): Present-day stress field in the Gibraltar Arc (westernMediterranean). J. Geophys. Res, 112: B08404, doi:10.1029/2006JB004683

Font, Y., H. Kao, S. Lallemand, C.-S. Liu, and L.-Y. Chiao (2004). Hypocentral determination offshore eastern Taiwan using the maximum intersection method, Geophys. J. Int. 158, 655–675.

Fukao, Y. (1973). Thrust faulting at lithospheric plate boundary. The Portugal earthquake of 1969. Earth Plan. Sci. Lett. 18, 205-216.

Grimison, N.L., Chen, W.P., 1988. Source mechanisms of four recent earthquakes along the Azores–Gibraltar plate boundary. Geophysical Journal 92, 391–401.

Hayward, N., Watts, A.B., Westbrook, G.K. and Collier, J.S. (1999): A seismic reflection and GLORIA study of compressional deformation in the Gorringe Bank region, eastern North Atlantic. Geophys. J. Int., 138: 831-850.

Horiuchi, S., H. Negishi, K. Abe, A. Kamimura, and Y. Fujinawa (2005). An automatic processing system for broadcasting system earthquake alarms, Bull. Seism. Soc. Am. 95 347–353.

Iannaccone G, Zollo A, Elia L, Convertito V, Satriano C, Martino C, et al. A prototype system for earthquake early-warning and alert management in southern Italy. Bull Earthquake Eng 2009, 10.1007/s10518-009-9131-8.

IGN (1983) Sismicidad del Area Ibero-mogrebí. Publicación 203. Presidencia del Gobierno.

Johnston, A. C. (1996). Seismic moment assessment of earthquakes in stable continental regions, III New Madrid 1811-1821, Charleston 1886 and Lisbon 1755. Geophys. J. Int., 126, 314-344.

Martínez Solares, J. M. and A. López Arroyo (2004). The great historical 1755 earthquake. Effects and damage in Spain. J. Seismol. 8, 275-294,

Morel, J.L. y Meghraoui, M. (1996): Goringe-Alboran-Tell tectonic zone: A transpression system along the Africa-Eurasia plate boundary. Geology, 24: 755–758.

Kanamori, H. (2005). Real-Time Seismology and Earthquake Damage Mitigation, Annu. Rev. Earth Planet. Sci., 33, 195--214 doi: 10.1146/annurev.earth.33.092203.122626.

Peng, H.S., Z.L. Wu, Y.M. Wu, S.M. Yu, D.N. Zhang, and W.H. Huang (2011). Developing a prototype earthquake early warning system in the Beijing Capital Region, Seism. Res. Lett. 82 394-403.

Pro, C., E. Buforn, M. Bezzeghoud, and A. Udías, (2013). The earthquakes of 29 July 2003, 12 February 2007, and 17 December 2009 in the region of Cape Saint Vincent (SW Iberia) and their relation with the 1755 Lisbon earthquake. Tectonophysics 583, 16-27, http://dx.doi.org/10.1016/j.tecto.2012.10.010.

Rydelek, P. and S. Horiuchi (2006). Earth science: is earthquake rupture deterministic? Nature 442 doi: 10.1038/nature0496 3.

Rydelek, P., C. Wu, and S. Horiuchi (2007). Comment on Earthquake magnitude estimation from peak amplitudes of very early seismic signals on strong motion records by Aldo Zollo, Maria Lancieri, and Stefan Nielsen. Geophys. Res. Lett. 34. doi: 10.1029/200 7GL029387.

Satriano, C., A. Lomax, and A. Zollo (2008). Real-Time Evolutionary Earthquake Location for Seismic Early Warning. Bulletin of the Seismological Society of America America 98.3, pp. 14821494. doi:10.1785/0120060159.

Satriano, C., Elia, L., Martino, C., Lancieri, M., Zollo, A., and Iannaccone, G. (2010). PRESTo, the earthquake early warning system for southern Italy: concepts, capabilities and future perspectives, Soil Dyn. Earthq. Eng. doi:10.1016/j.soildyn.2010.06.008.

Stich, D., F. Mancilla, S. Pondrelli, and J. Morales (2007). Source analysis of the February 12th 2007, Mw 6.0 Horseshoe earthquake: Implications for the 1755 Lisbon earthquake. Geophysical Research Letters 34. http://dx.doi.org/10.1029/2007GL0300127

Udías, A., López Arroyo, A., Mezcua, J., 1976. Seismotectonic of the Azores-Alboran region. Tectonophysics 31, 259–289.

Wald, D. et al. (1999). Relationships between Peak Ground Acceleration, Peak Ground Velocity, and Modied Mercalli Intensity in California. In: Earthquake Spectra 15.3, p. 557. doi: 10.1193/1.15 86058.

Wu, Y.M. and L. Zhao (2006). Magnitude estimation using the first three seconds P-wave amplitude in earthquake early warning, Geophys Res Lett. 33 L16312 doi:10.1029/2006GL026871.

Wu, Y.-M. and H. Kanamori (2005). Rapid Assessment of Damage Potential of Earthquakes in Taiwan from the Beginning of P -Waves. Bulletin of the Seismological Society of America America 95.3, pp. 1181-1185.doi:10.1785/0120040193.

Wu, Y.-M. and H. Kanamori (2008a). Development of an earthquake early warning system using real-time strong motion signals. Sensors 8, pp. 1-9.

Wu, Y.-M and H. Kanamori (2008b). Exploring the feasibility of on-site earthquake early warning using close-in records of the 2007 Noto Hanto earthquake. Earth Planets and Space 60, pp. 155-160.

Zollo, A., M. Lancieri, & Nielsen, S. (2006). Earthquake magnitude estimation from peak amplitudes of very early seismic signals on strong motion, Geophys Res Lett. 33, L23312 doi:10.1029/2006GL027795

Zollo, A., M. Lancieri, & Nielsen, S. (2007). Reply to comment by P. Rydelek et al. On Earthquake magnitude estimation from peak amplitudes of very early seismic signals on strong motion records. Geophysical Research Letters 34.20, pp. 1215. doi: 10.1029/2007GL030560.

Zollo, A, O. Amoroso, M. Lancieri, Y.M. Wu & Kanamori, H. (2010). A threshold-based earthquake early warning using dense accelerometer networks, Geophys J Int 183 963-974.

Zollo, A., S. Colombelli, L. Elia, A. Emolo, G. Festa, G. Iannaccone, C. Martino, and P. Gasparini (2014). An integrated regional and on-site Earthquake Early Warning System for Southern Italy: concepts, methodologies and performances, In “Early Warning for Geological Disasters - Scientific methods and current practices”, Eds Wenzel & Zschau, Springer.

Figures captions

Figure 1. Distribution of earthquake epicenters (M ≥ 3, period 1960-2014) taken from the Instituto Geográfico Nacional Data Base. Black circles correspond to shallow events (h<40km), grey squares to intermediate depth (40<h<150 km). Stars are the largest earthquakes. GB= Gorringe Bank, HS= Horsenhoe Scarp, SVC= Saint Vicente Cape, GC= Gulf of Cadiz, SG= Strait of Gibraltar.

Figure 2. (a) Example of RTLoc derived locations for an event mimicking the great 1755 Lisbon Earthquake (red star) for three triggered stations. The RTLoc solutions (dots) have different colors depending on their uncertainty (i.e., from green indicating the best solution, towards violet indicating the worst solutions). Triggered (orange triangles) and not-triggered (blue triangles) stations, P-wave (green line), and S-wave (red line) wavefronts are shown. (b) and (c), the same as (a), but correspond to the use of ten triggered stations for deriving the location and derived using two different sets of data.

Figure 3. Outline of the EEW procedure proposed for the Iberian Peninsula to deal with the seismic threat represented by the SVC and GC areas.

Figure 4. (a) Schematic illustration (horizontal plane) of a wavefront propagating across two stations, and the derivation of the inter-stations distance. (b) Example of the application of a simplified RTLoc where only solutions compatible with the ‘conditional’ EDT are shown (green dots) when one station (orange triangle) has triggered. The true location (red star) and the estimated direction of propagation of wavefronts (black line) are

also shown. (c) and (d), the same as (b), but at the moment when three and ten stations have triggered, respectively.

Figure 5. (a) Schematic illustration of the PGV estimation at not-triggered stations (yellow dots) given at least two triggered stations (green dots) and the interstation distance between them and the others. (b) Comparison of PGV for event #6 plotted both with respect to their epicentral distance (blue dots) and their interstation distance (red dots) together with Eq. (3) (blue line) and Eq. (2) (red lines). (c) Comparison between observed (white triangles) and predicted (black dots) PGVs. (d) Residuals computed between the observed and predicted PGVs.

Figure 6. (a) PGV-GMPE (black line) derived from the EEW relationship of Carranza et al. (2013), with the +/- one standard deviation curves (dashed lines) and the observed PGVs for event #6 (Table 1) whose epicenter is in the SVC region. (b) and (c) Distribution with distance and histogram, respectively, of the residual between the observed and predicted PGVs from the recordings of the seven events considered in this study (Table 1).

Figure 7. (a) I_{MM} derived from PGVs for a scenario mimicking the great 1755 Lisbon Earthquake. Seismic stations (triangles) are colored according to the I_{MM} scale of Wald et al. (1999). Target cities (black squares; Table 2). (b) I_{MM} at triggered stations from the SOS procedure (full colored triangles), and at not-triggered stations from the NOS procedure (contour colored triangles) at the time when three stations have triggered. (c) Distribution with distance of residuals between observed and predicted I_{MM} values. The stations have a different contour color depending if they are triggered (black) or not-triggered (red). (d) and (f), the same as (b), but for ten and fifty triggered stations, respectively, (e) and (g), the same as (c), but for ten and fifty triggered stations, respectively.

Figure 8. (a) The same as Figure (4a), but for event #3 (Table 1). (b) and (c) are the observed and EEW I_{MM} values, respectively. The same symbols as in Figure (7) are used.

Figure 9. The same as Figure (8), but for event #7 (a, b, and c), and event #1 (d, e, and f) of Table (1).

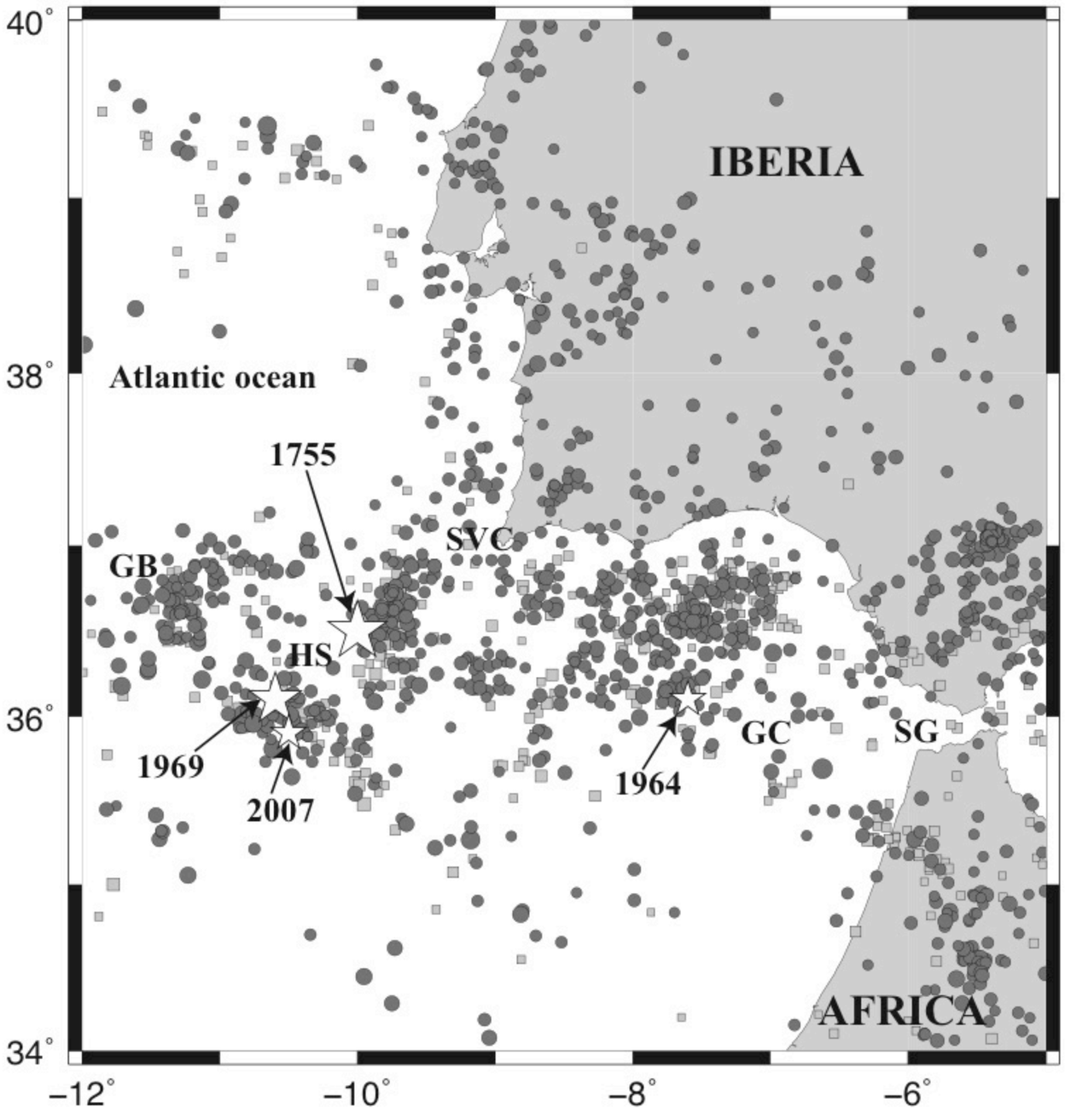
40°
38°
36°
34°
−12°
−10°
−8°
−6°
Atlantic ocean
IBERIA
AFRICA
1755
1969
2007
1964
SVC
GB
HS
GC
SG

Figure 1

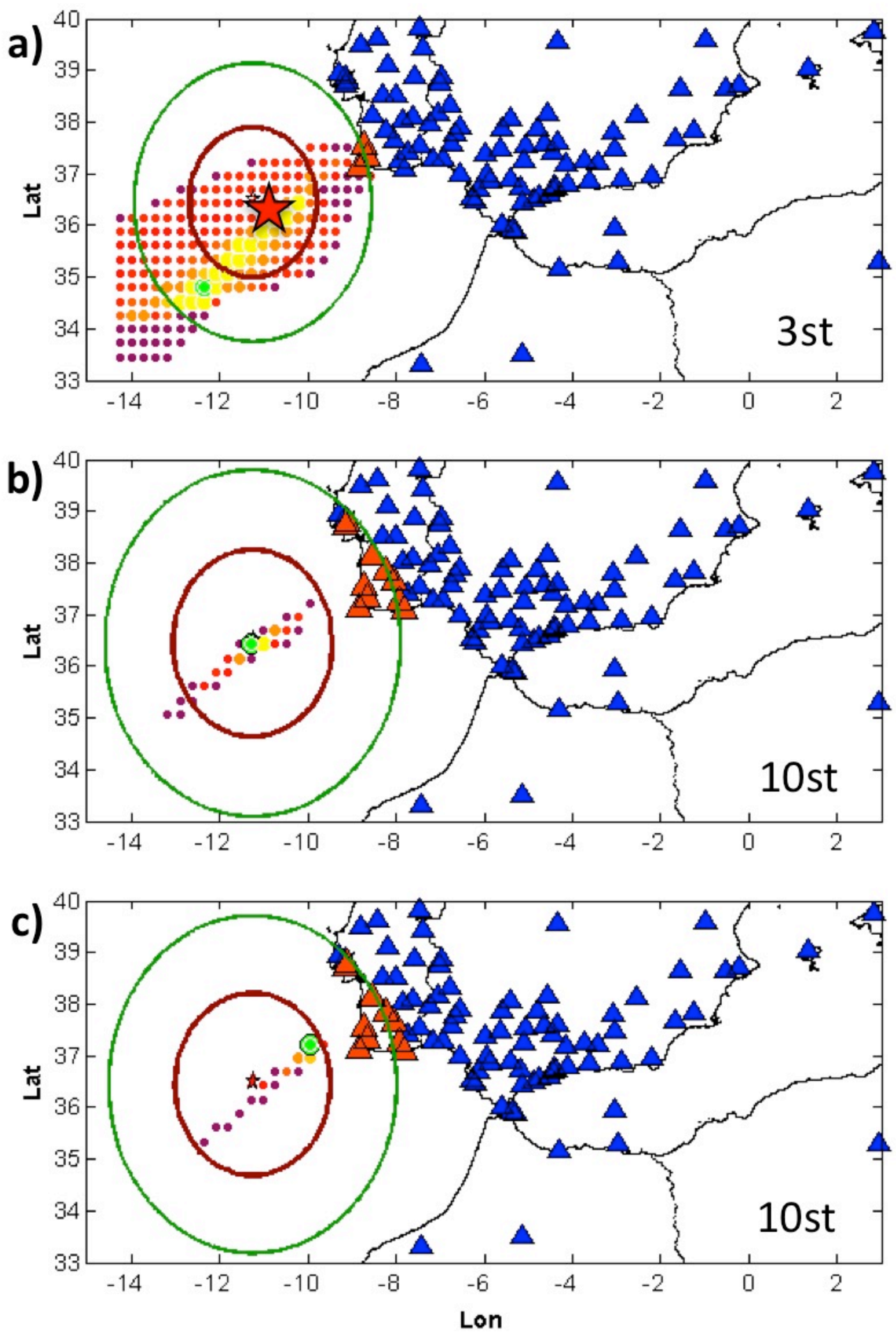

Figure 2

Figure 3

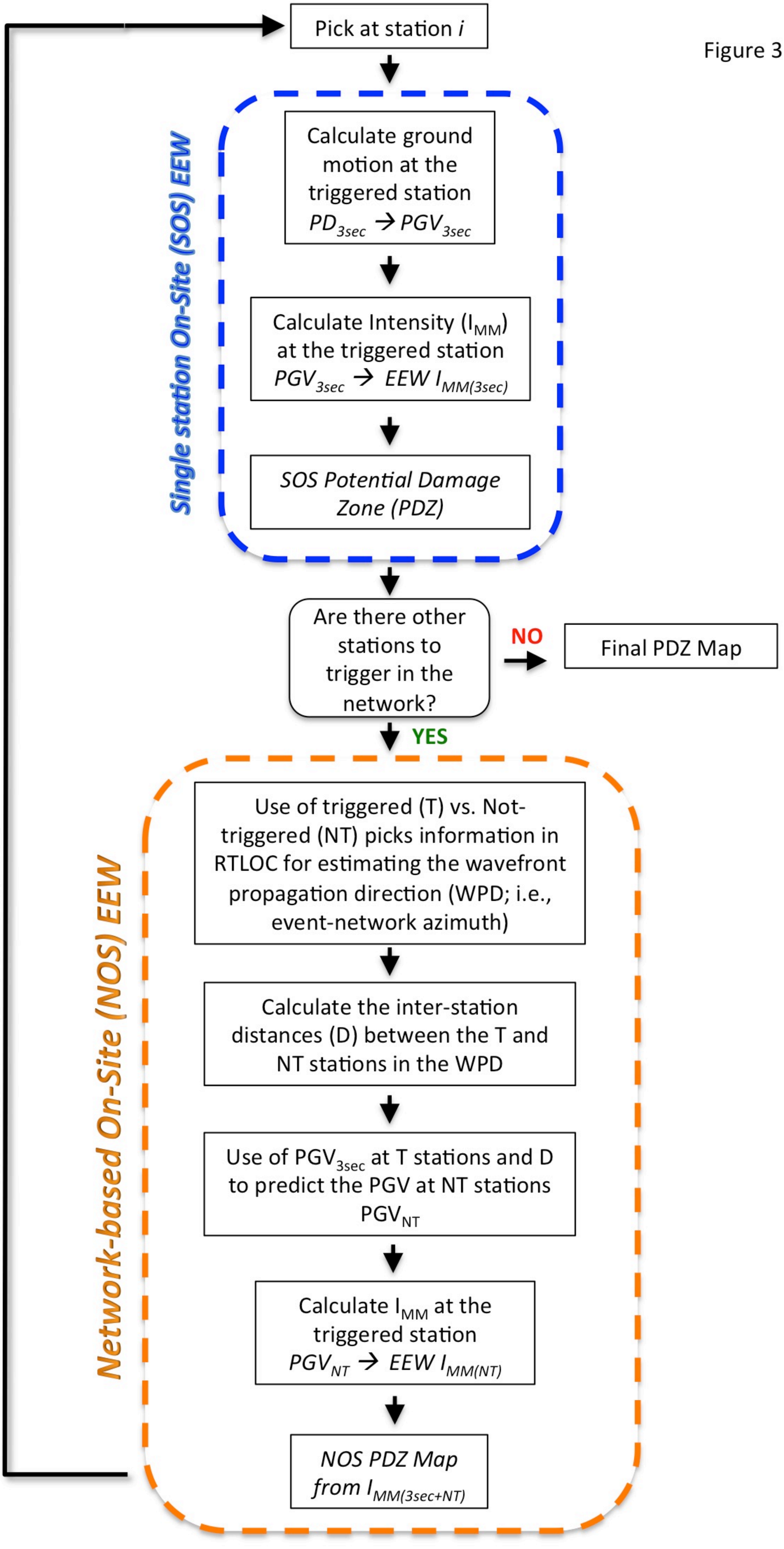
Pick at station *i*
Single station On-Site (SOS) EEW
Calculate ground motion at the triggered station
$PD_{3sec} \rightarrow PGV_{3sec}$
Calculate Intensity (I_{MM}) at the triggered station
$PGV_{3sec} \rightarrow$ *EEW* $I_{MM(3sec)}$
SOS Potential Damage Zone (PDZ)
Are there other stations to trigger in the network?
NO
Final PDZ Map
YES
Network-based On-Site (NOS) EEW
Use of triggered (T) vs. Not-triggered (NT) picks information in RTLOC for estimating the wavefront propagation direction (WPD; i.e., event-network azimuth)
Calculate the inter-station distances (D) between the T and NT stations in the WPD
Use of PGV_{3sec} at T stations and D to predict the PGV at NT stations PGV_{NT}
Calculate I_{MM} at the triggered station
$PGV_{NT} \rightarrow$ *EEW* $I_{MM(NT)}$
NOS PDZ Map from $I_{MM(3sec+NT)}$

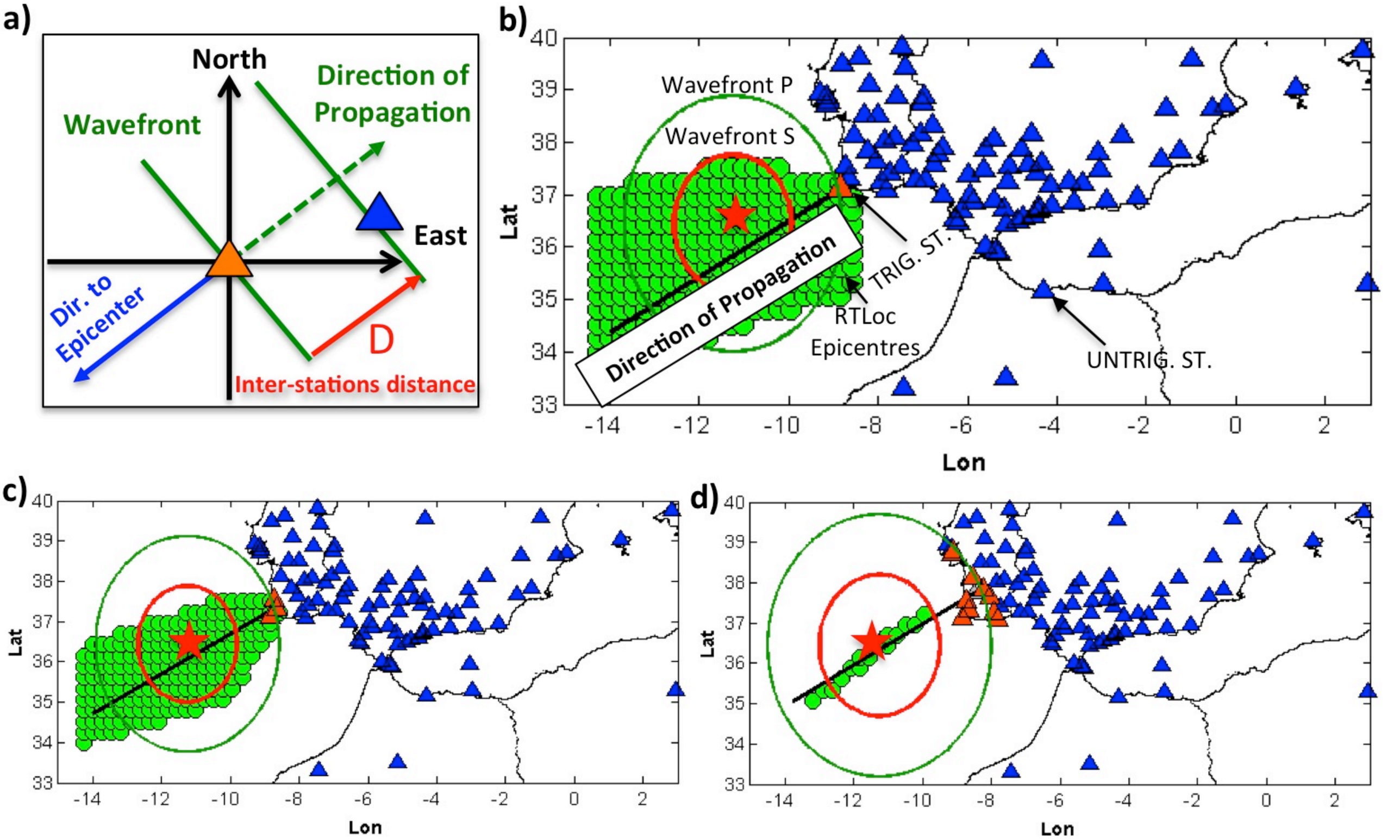
a)
North
Direction of Propagation
Wavefront
East
Dir. to Epicenter
D
Inter-stations distance
b)
Wavefront P
Wavefront S
Direction of Propagation
TRIG. ST.
RTLoc Epicentres
UNTRIG. ST.
Lat
Lon
c)
d)

Figure 4

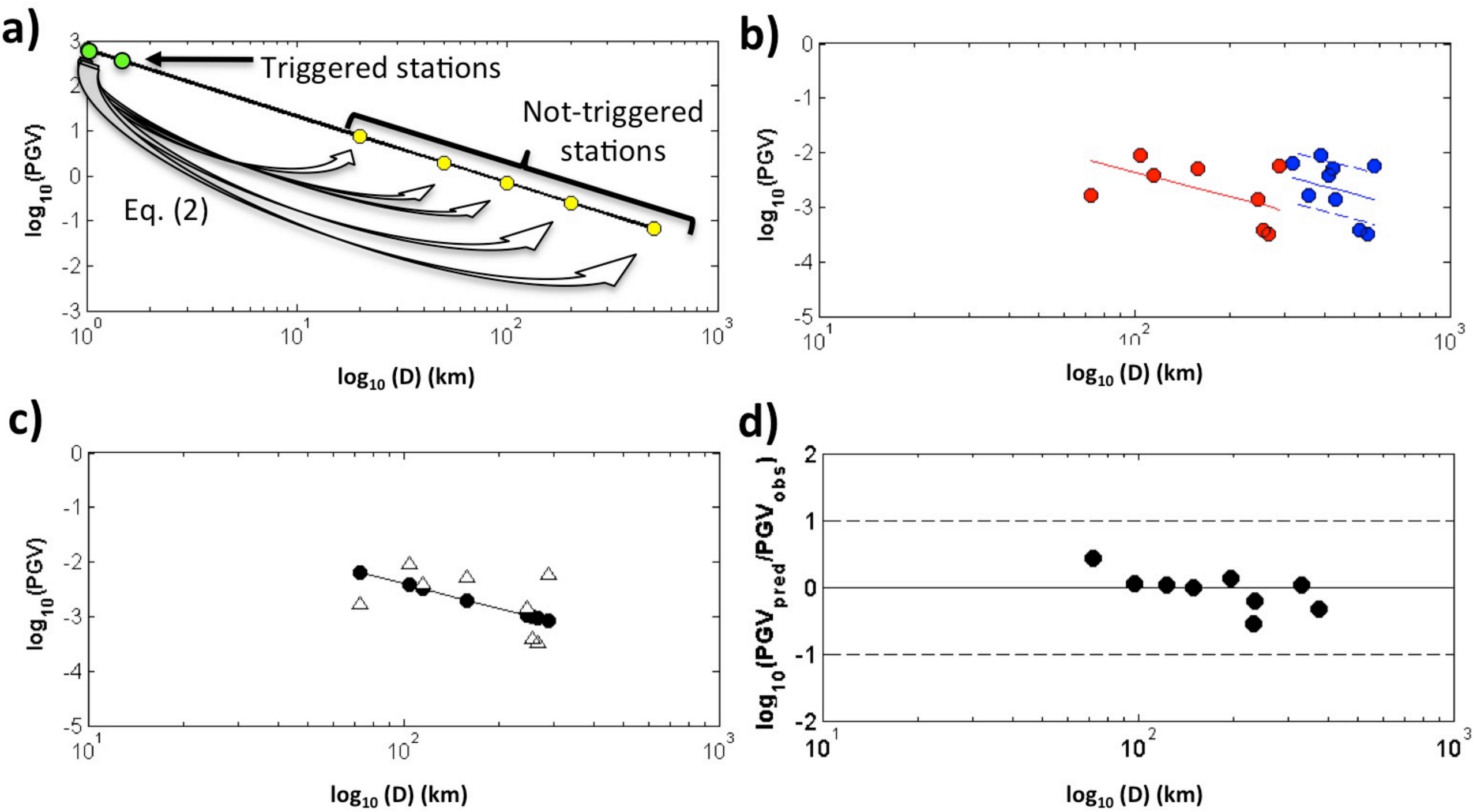
a)
Triggered stations
Not-triggered stations
Eq. (2)
log10(PGV)
log10 (D) (km)
b)
log10(PGV)
log10 (D) (km)
c)
log10(PGV)
log10 (D) (km)
d)
log10(PGVpred/PGVobs)
log10 (D) (km)

Figure 5

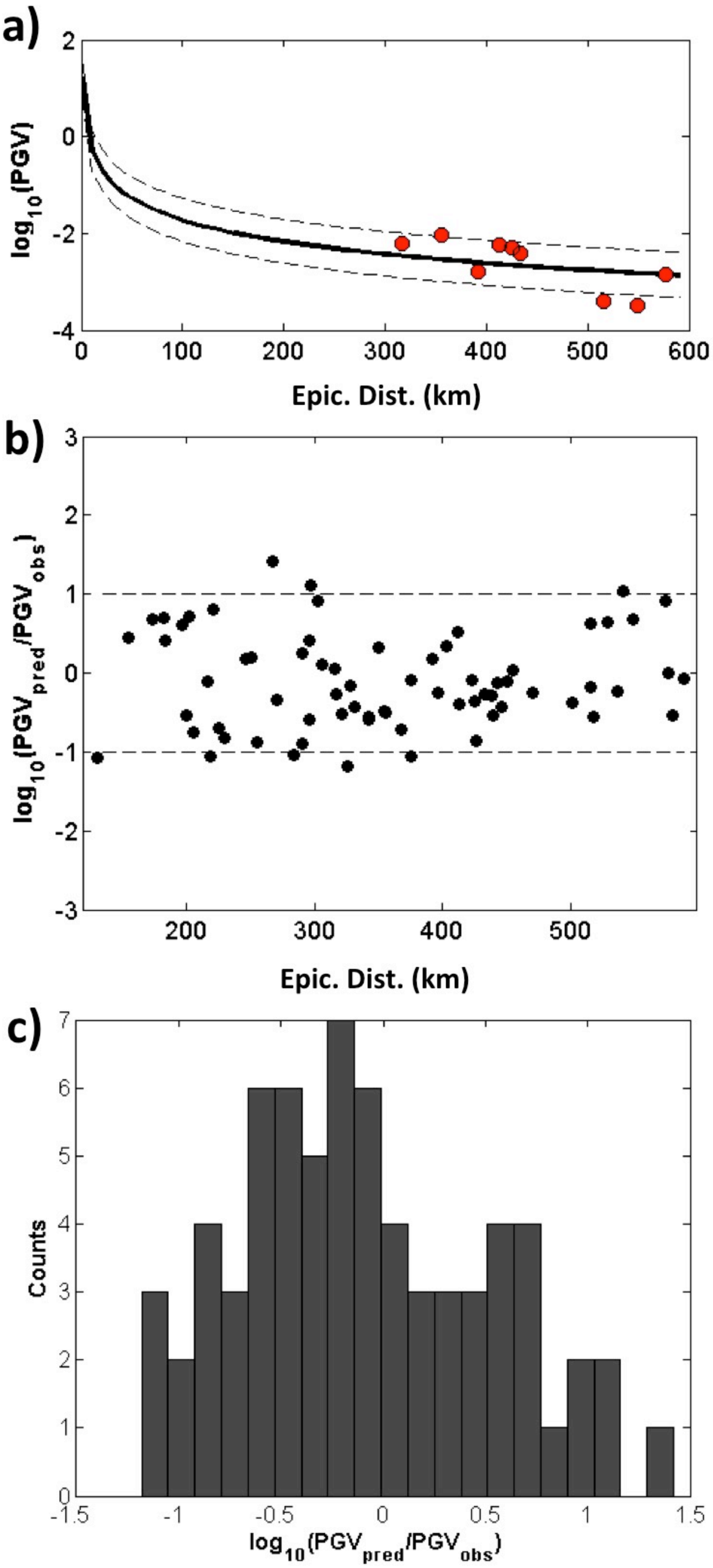
a)
log10(PGV)
Epic. Dist. (km)
b)
log10(PGVpred/PGVobs)
Epic. Dist. (km)
c)
Counts
log10(PGVpred/PGVobs)

Figure 6

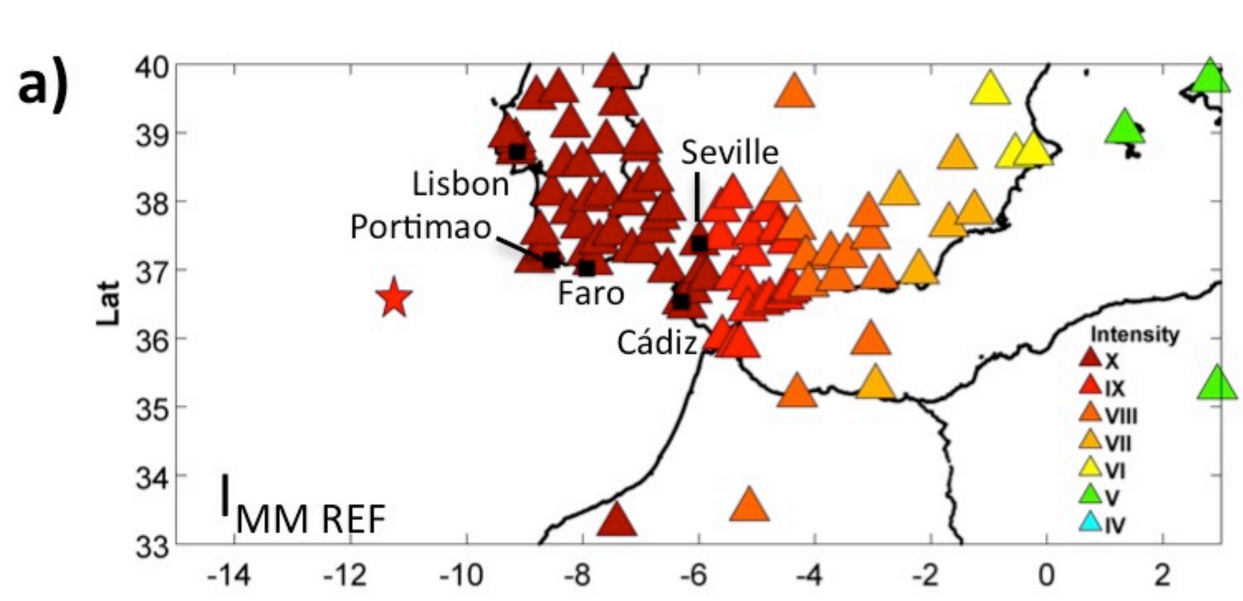
a)
Seville
Lisbon
Portimao
Faro
Cádiz
I MM REF
Intensity
X
IX
VIII
VII
VI
V
IV
Lat

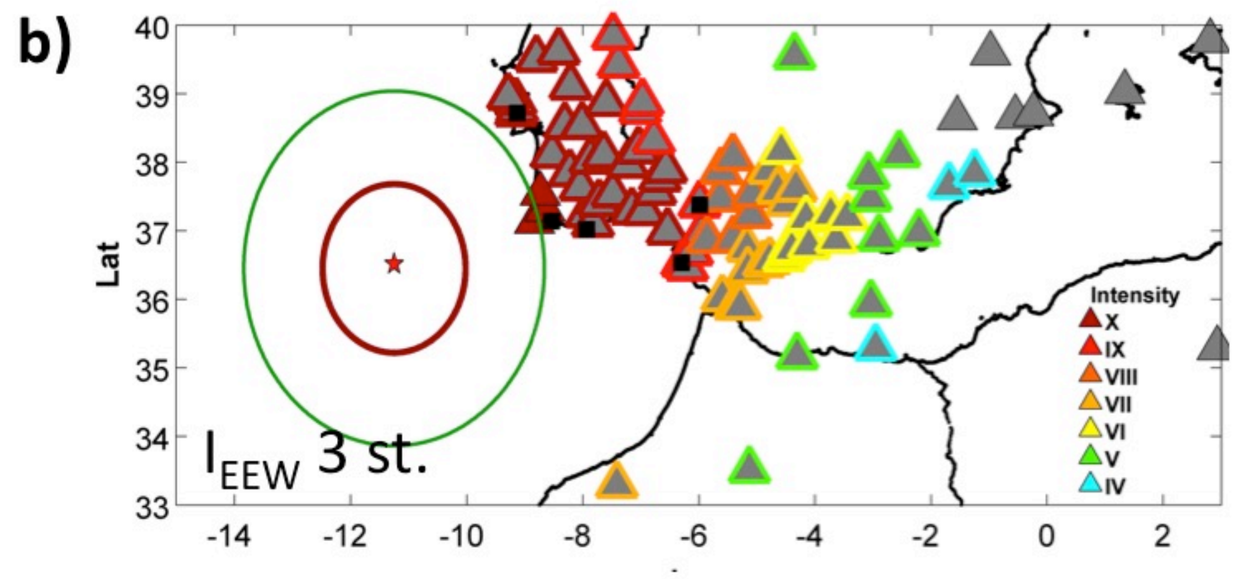
b)
I EEW 3 st.
Intensity
X
IX
VIII
VII
VI
V
IV
Lat

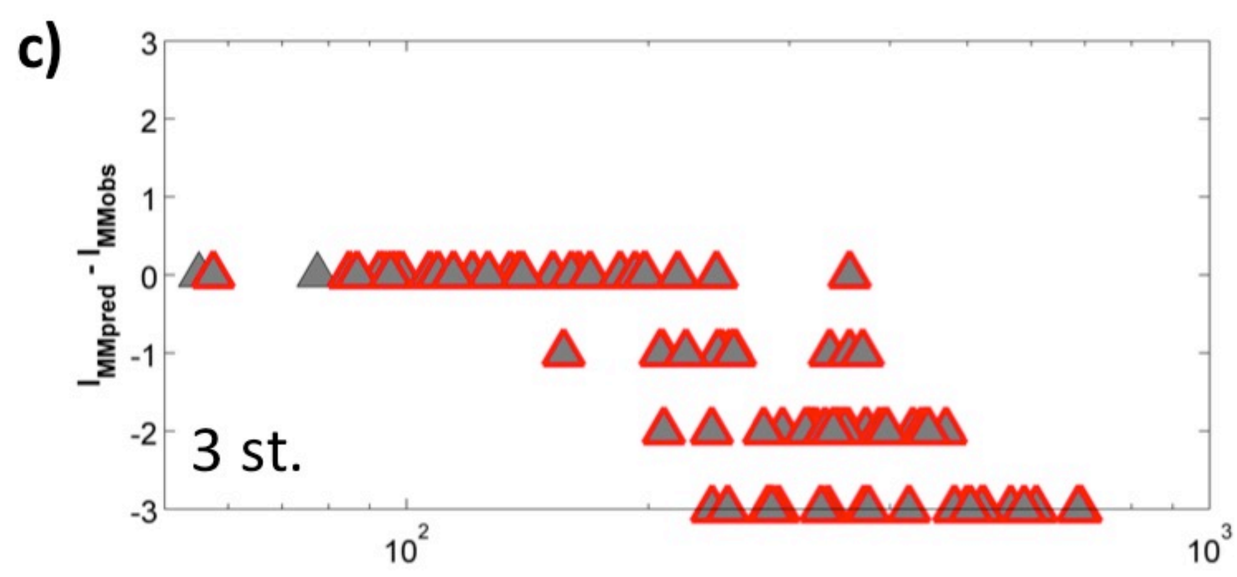
c)
3 st.
I MMpred - I MMobs

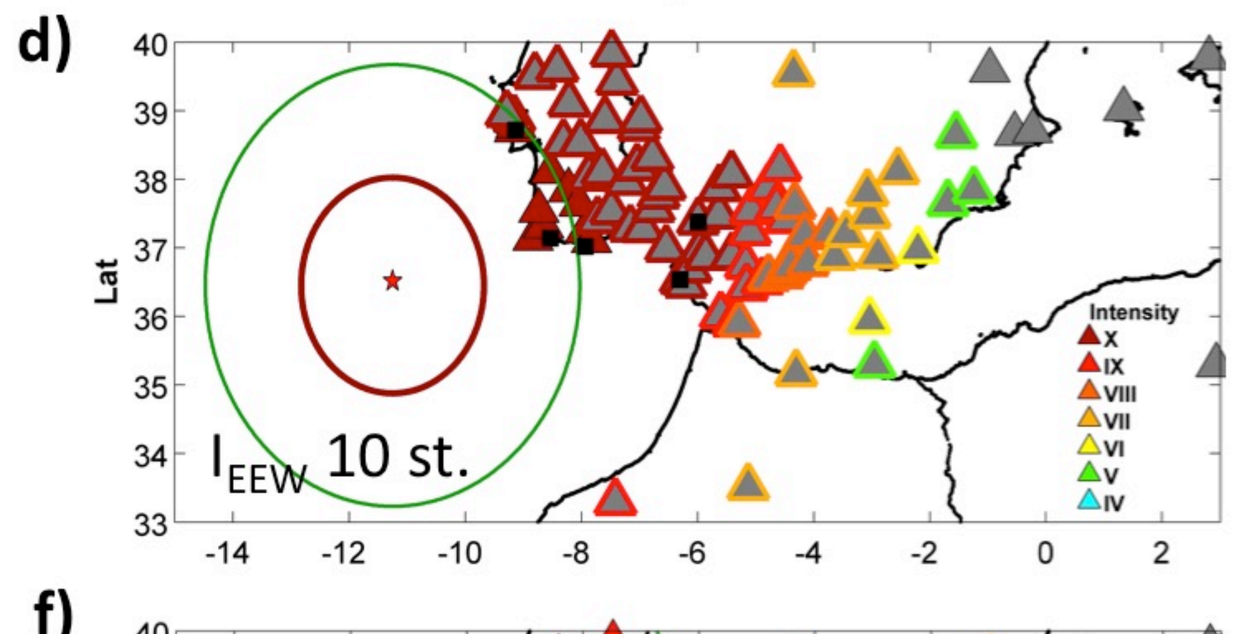
d)
I EEW 10 st.
Intensity
X
IX
VIII
VII
VI
V
IV
Lat

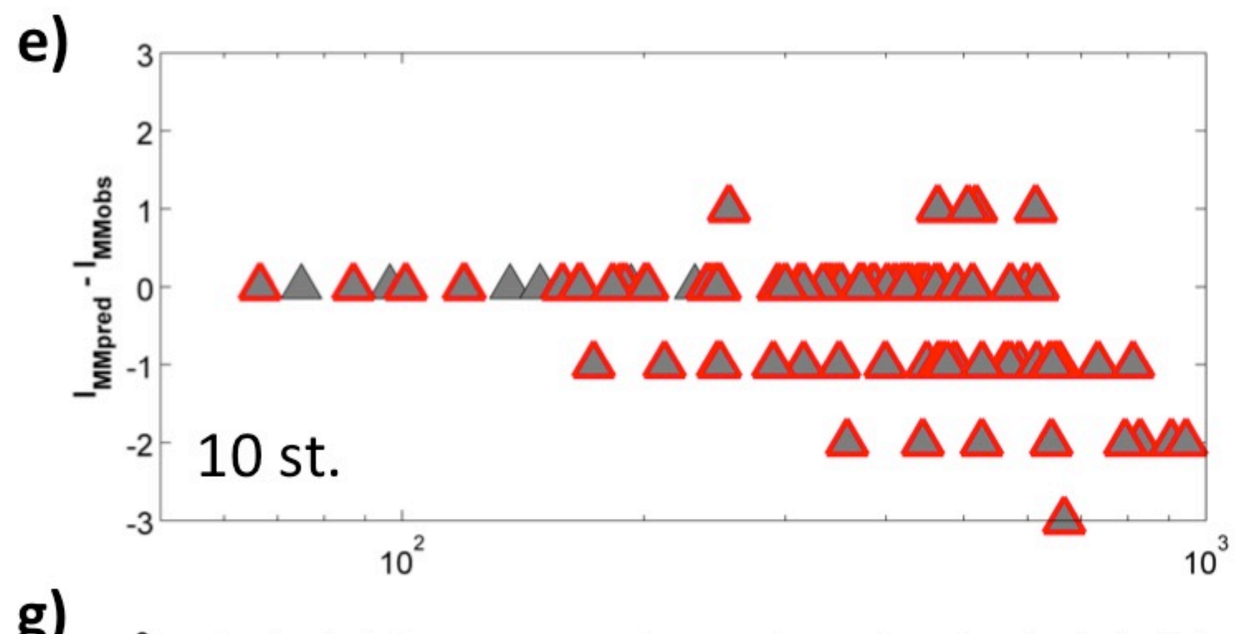
e)
10 st.
I MMpred - I MMobs

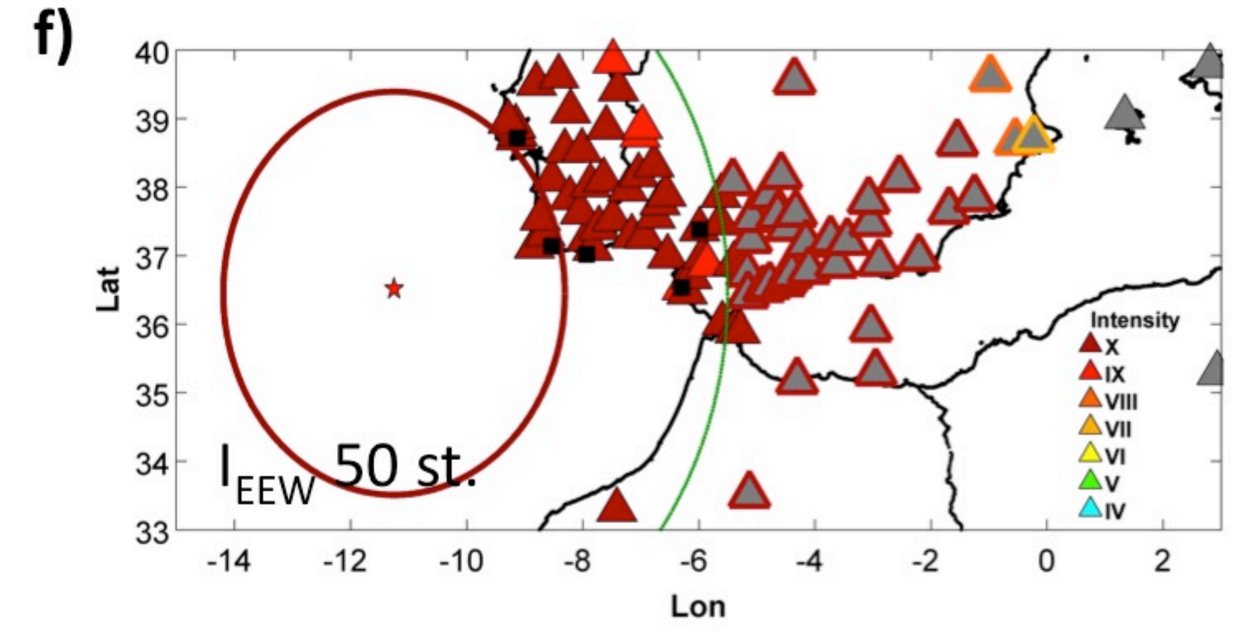
f)
I EEW 50 st.
Intensity
X
IX
VIII
VII
VI
V
IV
Lat
Lon

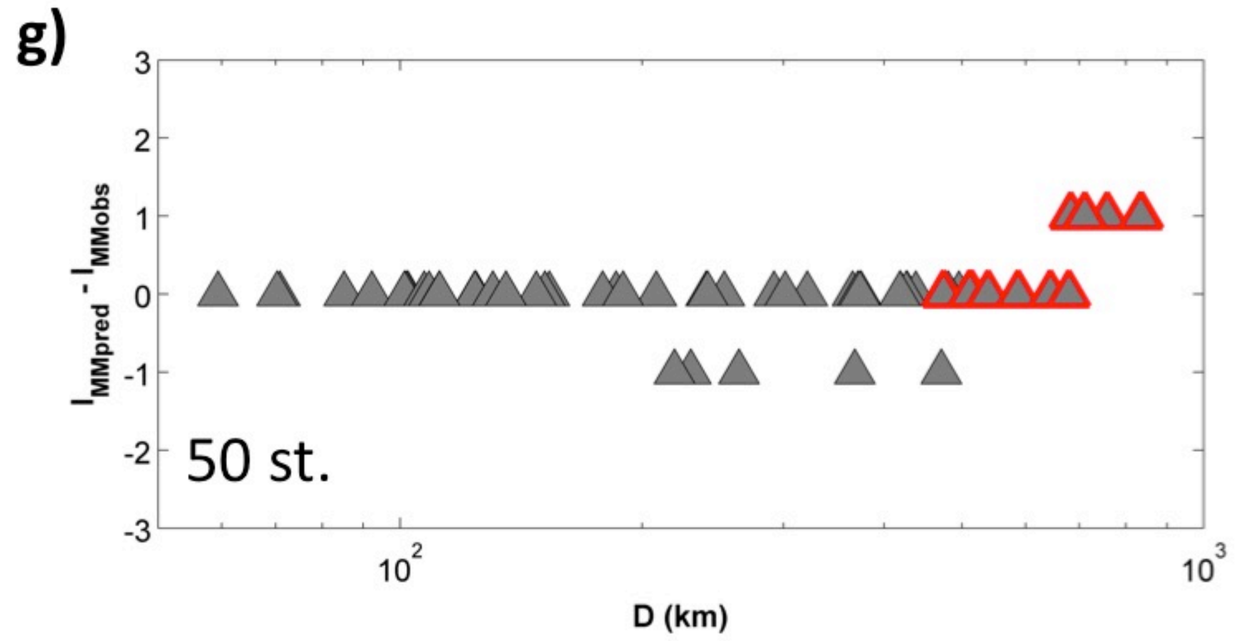
g)
50 st.
I MMpred - I MMobs
D (km)

Figure 7

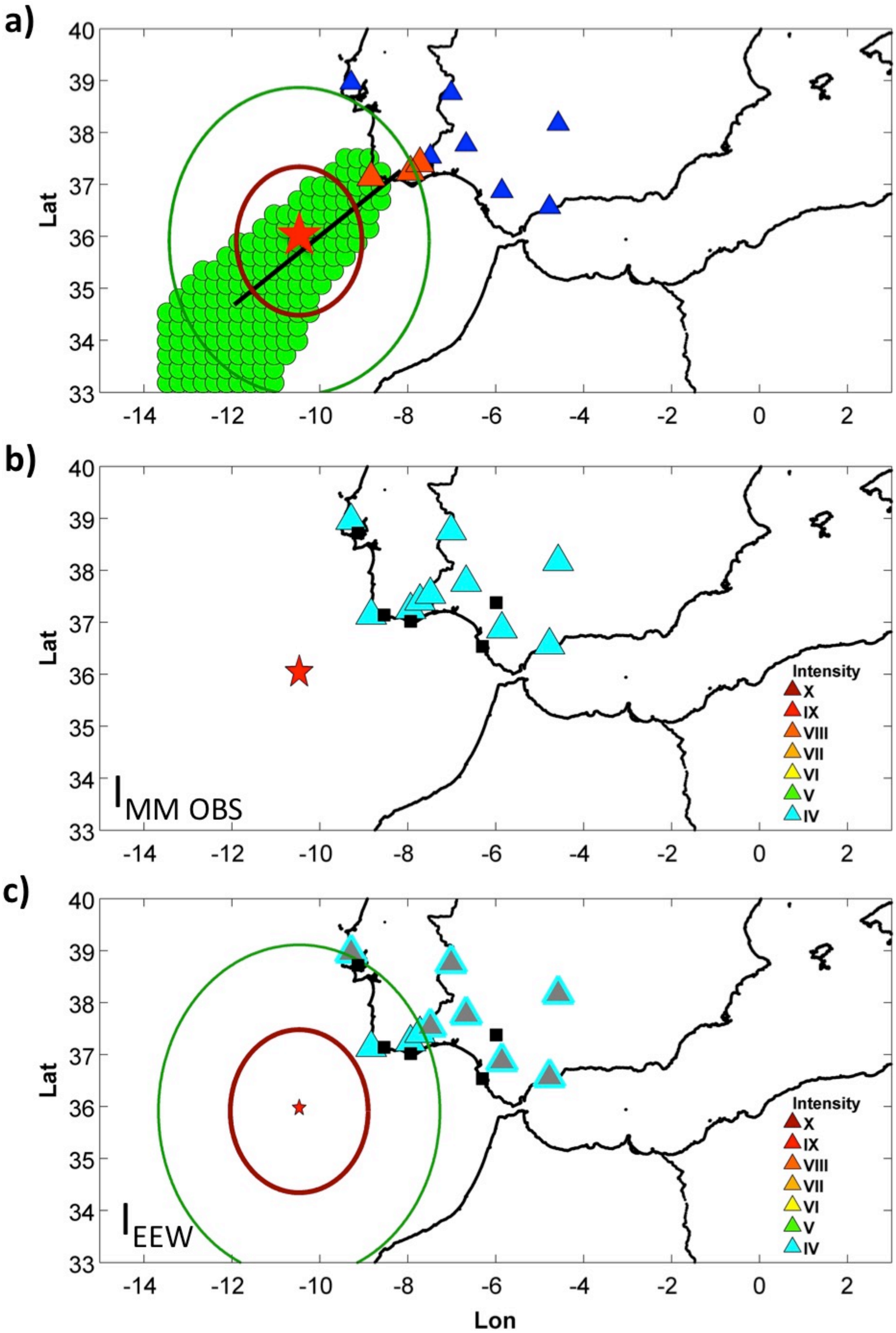
a)
b)
c)
Lat
Lon
40
39
38
37
36
35
34
33
-14
-12
-10
-8
-6
-4
-2
0
2
I MM OBS
I EEW
Intensity
X
IX
VIII
VII
VI
V
IV

Figure 8

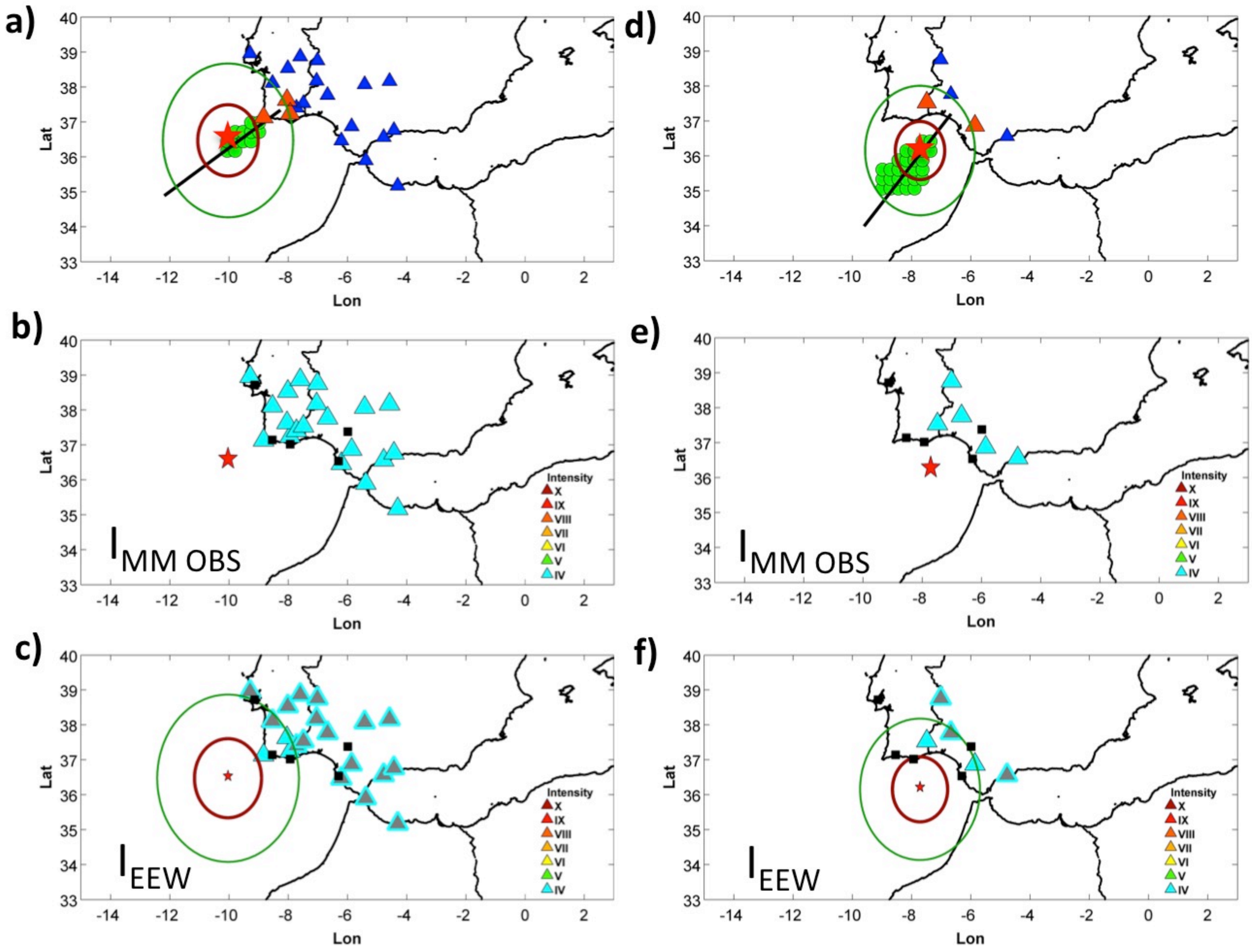

Figure 9